J. Fluid Mech. (2007), *vol.* 581, *pp.* 79–95.
doi:10.1017/S0022112007005708 Printed in the United Kingdom

On the extraction of gas from multilayered rock

ADRIAN FARCAS AND ANDREW W. WOODS

BP Institute for Multiphase Flow, University of Cambridge, Cambridge, CB3 0EZ, UK

(Received 5 May 2006 and in revised form 5 December 2006)

This paper presents some simple analytical and numerical models which describe the dynamics of gas flowing from a multilayered low-permeability porous rock into a fracture. The models account for the vertical flow between relatively high- and low-permeability layers. The motion of gas in a permeable rock is governed by a nonlinear diffusion equation for the gas pressure. We analyse the gas flow described by this equation in both bounded and unbounded domains. In both cases simple scalings laws are developed to determine the fluxes and the dimensions of the regions within the rock which may be depleted over a given time scale. These are compared with the results of a full numerical model.

1. Introduction

Much work has been carried out to quantify liquid and gas flow through permeable strata (e.g. Bear 1972; Dagan 1989) owing to their great industrial and environmental importance. Although a complete description of such flows often involves complex, multiphase flow relations which require numerical solution, there is considerable value in developing approximate models which admit simplified or approximate analytic solutions (Barenblatt 1996). The present work is concerned with developing some approximate analytic and numerical models to describe the extraction of gas from a porous medium composed of two layers of different thickness and permeability. This problem is of growing interest to the natural-gas industry owing to the progressive depletion of gas reservoirs and the extraction of gas from increasingly impermeable layers. In many such reservoirs of low-permeability rock, the rock near the well may hydraulically fractured during drilling. The objective of generating such fractures is to enhance the flow by providing a large surface to which the gas can drain from the reservoir; it then flows along the relatively high-permeability fracture and into the well (figure 1).

The pressure-driven isothermal flow of gas, with equation of state $P = \rho RT$, relating pressure P, density ρ, gas constant R and temperature T, and with viscosity μ that does not depend on pressure, in a porous layer of permeability k and porosity ϕ is governed by the relation

$$P_t = \frac{k}{\phi\mu}\nabla(P\nabla P) \tag{1.1}$$

Equation (1.1) was first derived by Leibenzon (1929) and later by Muskat & Botset (1931). The detailed formulation of the isothermal gas filtration problem can be found in Barenblatt, Entov & Ryzhik (1990).

We analyse the flow described by this equation in bounded and unbounded domains consisting of two layers of different permeability. In both cases we present simple

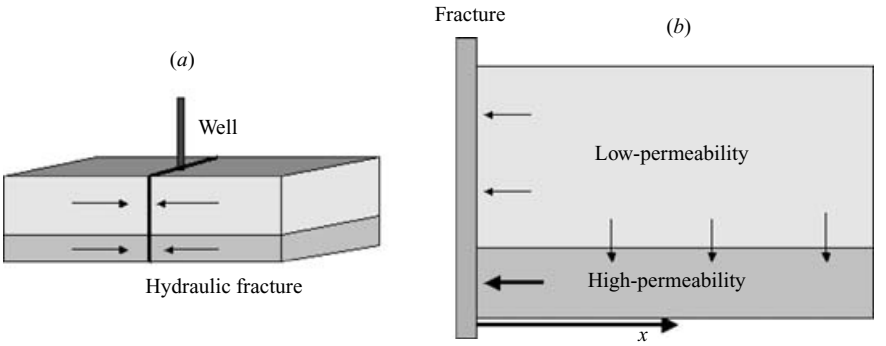

FIGURE 1. (*a*) A vertical well with an engineered hydraulic fracture. (*b*) Quasi-one-dimensional draining of gas into the fracture.

scaling laws for determining the fluxes and the dimensions of the regions within the domain which may be depleted over a given time scale.

2. One-layer considerations

Let us concentrate first on the decompression-driven flow of gas from a thin laterally extensive reservoir into a planar vertical fracture. In this case, the flow is essentially one-dimensional, varying with the normal distance x from the fracture (figure 1), and so described by the equation

$$P_t = \frac{k}{\phi\mu}(PP_x)_x. \tag{2.1}$$

We consider a reservoir having lateral extent L from the reservoir and initial gas pressure $P_{max} = P(L, 0)$ at the far end $x = L$. It is useful to introduce the effective diffusion coefficient $\alpha = k(P_{max})/\phi\mu$, and the cross-reservoir diffusion time $t_D = L^2/\alpha$. In order to non-dimensionalize the space and time quantities we consider h_{ref} and α_{ref}, say the thickness and diffusivity of a reference layer, and we scale $\alpha' = \alpha/\alpha_{ref}$, $x' = x/h_{ref}$, $L' = L/h_{ref}$, $t'_D = t_D/t_{Dref}$, and $t' = t/t_{Dref}$ where $t_{Dref} = h_{ref}^2/\alpha_{ref}$. We also introduce the dimensionless pressure $p(x', t') = P(x, t)/P_{max}$. The mass flux per unit area of the fracture

$$Q(t) = \frac{k}{\mu}\rho(0, t)P_x(0, t) \tag{2.2}$$

can be scaled as $q(t') = Q(t)/Q_{ref}$, where $Q_{ref} = \phi P_{max}/h_{ref}R_gT$.

For convenience, we drop the primes for the remainder of this section. Then equation (2.1) may be expressed as

$$p_t = \alpha\,(pp_x)_x \tag{2.3}$$

and the flux (2.2) becomes

$$q(t) = \alpha p(0, t)p_x(0, t). \tag{2.4}$$

The first exact solutions for the nonlinear equation (2.3) were presented by Boussinesq (1904) and a review of these can be found in Bear (1972). Boussinesq has shown that equation (2.3) with the set of initial and boundary conditions

$$p(x, 0) = p_{init}(x), \tag{2.5}$$

$$p(0, t) = 0, \quad \partial p/\partial x|_{x=L} = 0, \tag{2.6}$$

has the separable solution

$$p(x,t) = f(t)g(x), \tag{2.7}$$

where $f(t)$ given by

$$f(t) = \frac{f(0)}{1 + cf(0)\alpha/L^2}; \quad c = 3a^2/2, \quad a = \int_0^1 \frac{\tau\,\mathrm{d}\tau}{\sqrt{1-\tau^3}} = \tfrac{1}{3}B(1/2, 2/3) \approx 0.862, \tag{2.8}$$

and $g(x)$ is given by

$$x = \frac{L}{a}\int_0^{g(x)} \frac{\tau\,\mathrm{d}\tau}{\sqrt{1-\tau^3}}; \quad x \leqslant L, \quad g(x) \leqslant 1, \quad g(1) = 1. \tag{2.9}$$

Using that $\lim_{x\to 0} g(x)g(x) = a$, the mass flux (2.4) can be rewritten for the separable solution (2.7) as

$$q_{sep}(t) = a\alpha\left[\frac{f(0)}{1 + cf(0)(\alpha/L^2)t}\right]^2. \tag{2.10}$$

A second Boussinesq solution of (2.3) can be obtained (Bear 1972) by introducing the variable $\eta = x/2(\alpha t)^{1/2}$ and assuming an unbounded domain ($L \to \infty$) and the initial condition

$$p(x,0) = 1. \tag{2.11}$$

In this case the problem admits a similarity solution $p(\eta)$ where $p(\infty) = 1$, $p(0) = p_0$ and

$$pp'' + (p')^2 + 2\eta p' = 0, \quad \text{for } \eta \geqslant 0. \tag{2.12}$$

The mass flux can be then expressed in terms of the similarity solution $p(\eta)$ as

$$q_{sim}(t) = \tilde{a}\left(\frac{\alpha}{t}\right)^{1/2}, \tag{2.13}$$

where $\tilde{a} = \frac{1}{2}p(0)p'(0)$, for $p(0) > 0$. In the special case when $p(0) = 0$, then $\tilde{a} = \frac{1}{2}\lim_{\eta\to 0} p(\eta)p'(\eta) \approx 0.33$.

It should be noted that the similarity solution $p(\eta)$ applies to an unbounded domain $(0, \infty)$. In practice, the domain is bounded, i.e. $(0, L)$. In this situation, the large-time asymptotic behaviour of $p(x,t)$ is towards the separable solution (2.7) (Aronson & Peletier 1981). However, at early times $t \ll t_D$, i.e. before the pressure signal has reached the far boundary of the reservoir, it is reasonable to approximate the domain as unbounded. Figure 2(*a*) presents several numerical pressure profiles p_{num} obtained by solving numerically the partial differential equation (2.3) in the domain $(0, 1)$ with the boundary conditions $p(0,t) = 0$ and $p_x(1,t) = 0$ and the initial condition (2.11). The diffusion coefficient was taken as $\alpha = 1$; hence the diffusion time $t_D = 1$. It can be seen from figure 2(*a*) that the numerical pressure profiles p_{num} are very well approximated by the similarity solution profiles p_{sim} for $0 < t < 0.15t_D$. However, after this initial period, the numerical solution is very well approximated by the separable solution p_{sep} with $cf(0) \simeq 1.2696$. Figure 2(*b*) presents the evolution in time of the error norms defined as

$$\|p_{num} - p_{sim}\|_2^2 / \|p_{num}\|_2^2$$

and

$$\|p_{num} - p_{sep}\|_2^2 / \|p_{num}\|_2^2, \quad \text{where } \|p\|_2^2 = \int_0^L |p(x)|^2\,\mathrm{d}x.$$

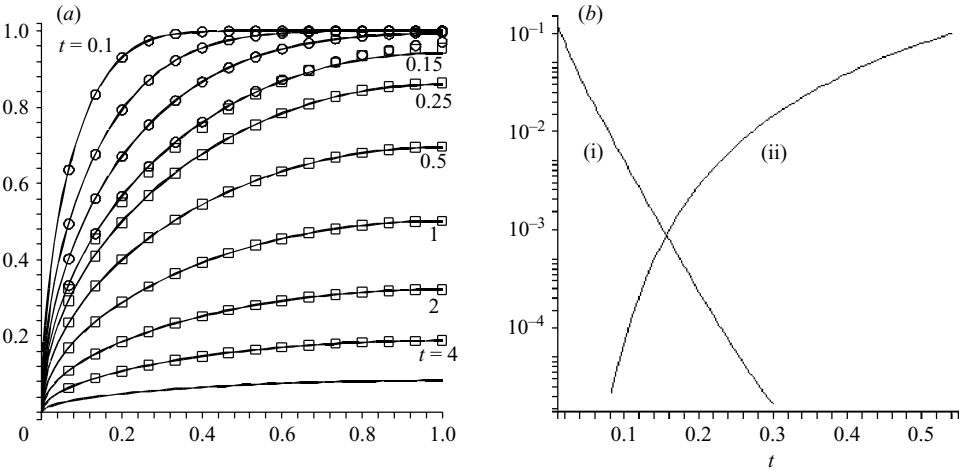

FIGURE 2. (*a*) Numerical pressure profiles p_{num} (——) compared with the similarity solution profiles p_{sim} (○ ○ ○) and the separable solution profiles p_{sep} (□ □ □) for the test example from § 2.1. (*b*) The evolution of the normalized error norms (i) $\|p_{num} - p_{sep}\|_2^2 / \|p_{num}\|_2^2$ and (ii) $\|p_{num} - p_{sim}\|_2^2 / \|p_{num}\|_2^2$.

It can be seen from figure 2 that there is a swift switch between the similarity solution and the separable solution at $t \simeq 0.15 t_D$. At this time, the pressure at the far boundary of the reservoir has value $p(1, t) \simeq 0.94$. The observed value of $cf(0)$ means that $f(0) \simeq 1.138$ so that the initial condition $p(x, 0) = 1$ is equivalent to a virtual initial condition of separable shape $p_{init} = f(0)g(x)$, with $p(L, 0) = 1.138$.

3. Analogue Hele-Shaw draining experiments

Leibenzon (1929) discovered that the isothermal gas filtration equation (1.1) is similar to the equation obtained by Boussinesq (1904) for the distribution of the hydraulic head in gently sloping unconfined groundwater flow, namely

$$h_t = \frac{gk\rho}{\phi\mu} \frac{\partial}{\partial x}\left(h \frac{\partial h}{\partial x}\right). \tag{3.1}$$

Furthermore, these similar flows have been simulated using Hele-Shaw analogue experiments, see e.g. Shestakov (1956) and Barenblatt *et al.* (1990) for more details.

To test the theoretical predictions of the flux, we have carried out a series of draining experiments using a vertical Hele-Shaw cell 15 cm high, $L = 27$ cm long and with a gap width of $d = 3$ mm (cf. King & Woods 2003). The cell was placed on a horizontal surface, and a layer of golden syrup, $h_0 = 9$ cm deep, filled the length of the cell.

At the start of the experiment, a gate at one end of the cell was removed so that syrup could then drain freely from the end of the cell. The syrup was collected in a vessel placed on a digital mass balance to record the mass that issued from the cell, $M(t)$, as a function of time. Figure 3 shows a typical data set $M(t)$ as a function of time t from an experiment. The separable solutions presented above suggest that for time $t > 0.15 t_D$ the draining flux should vary according to the form

$$\frac{\mathrm{d}M}{\mathrm{d}t} = a \frac{M_0}{t_D} \left(\frac{f(0) t_D}{t_D + cf(0)t}\right)^2, \tag{3.2}$$

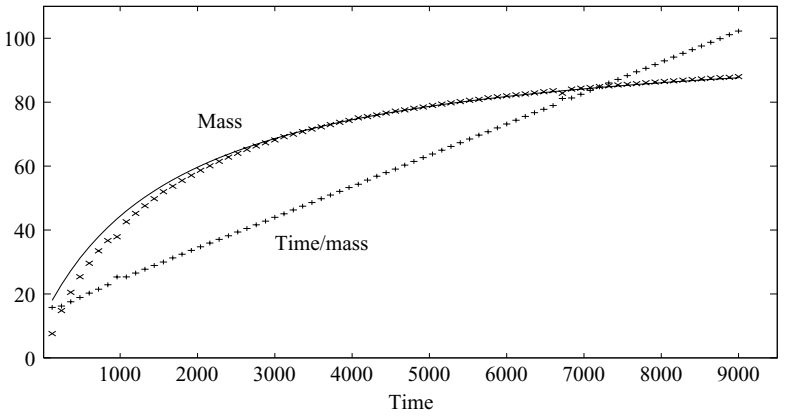

FIGURE 3. Experimental results: the mass of the syrup issuing from the cell $M(t)$ in grams ($\times\ \times\ \times$) compared with the separable prediction (——), and the quantity $t/M(t)$ ($+\ +\ +$) plotted as a function of time.

where M_0 is the initial mass of syrup in the cell and all the quantities are now dimensional. We have plotted the data in the form $t/M(t)$ as a function of time since the separable prediction for the collected mass,

$$M(t) = M_0\left(1 - \frac{f(0)t_D}{t_D + cf(0)t}\frac{a}{c}\right), \tag{3.3}$$

suggests that at long time, $t \gg 0.15t_D$, the quantity $t/M(t)$ should asymptote to a line of slope $1/M_0$ and intercept $t_D/cf(0)M_0$. As seen in figure 3, the data are in excellent accord with this prediction. The slope of the asymptote indicates a mass $M_0 = 102\,\mathrm{g}$ which when correlated with the intercept gives the diffusion time $t_D = 2330\,\mathrm{s}$. These results are consistent with the predictions $M_0 = \rho L h_0 d$ and $t_D = L^2\mu/\rho g k h_0$, respectively, with syrup of viscosity 30 Pa s and density $1410\,\mathrm{kg\,m^{-3}}$, and a cell of permeability $k = d^2/12$.

4. Two layers

4.1. *Unbounded domain*

We now extend the model to include two or more layers of different permeability. In this situation, the gas tends to diffuse more rapidly along high-permeability layers and it also drains from the low-permeability layers into the adjacent high-permeability layers. For simplicity, let us initially consider the case of two layers with permeabilities k_1 and k_2 and respective widths h_1 and h_2 (cf. figure 1). We assume that $k_2 < k_1$, so that the first layer tends to decompress more rapidly than the second and the inter-layer gas flow involves gas diffusing from the low-permeability second layer into the high-permeability first layer. We non-dimensionalize the quantities of interest, as done in § 2, with the particular choice of the first layer as the reference layer, i.e. we take $h_{ref} = h_1$ and $\alpha_{ref} = \alpha_1$. Therefore we have $h_1' = 1$, $\alpha_1' = 1$, and $h_2' = H$, $\alpha_2' = K$, where we denote the layer thickness and permeability ratios by $H = h_2/h_1$ and $K = k_2/k_1$. For convenience, we again drop the primes for the remainder of this section.

At early stages when diffusion across the low-permeability layer is negligible, $t \ll H^2/K$, the total flux can be approximated using (2.13) as

$$q_E \simeq \tilde{a}\left[\left(\frac{1}{t}\right)^{1/2} + H\left(\frac{K}{t}\right)^{1/2}\right]. \tag{4.1}$$

Thus the ratio of the fluxes from layer 1 and from layer 2 into the well is approximated by

$$\frac{q_{E2}}{q_{E1}} \simeq H\sqrt{K}. \tag{4.2}$$

At later stages, after the diffusion across the low-permeability layer becomes effective, $t \gg H^2/K$, it can be assumed that the pressure across the two layers gradually equilibrates and therefore the ratio of fluxes from layer 1 and from layer 2 at late times into the well is approximated by

$$\frac{q_{L2}}{q_{L1}} \simeq HK. \tag{4.3}$$

Since the fluxes again scale as $t^{-1/2}$, we can write $q_{L1} = q_{E1}/\beta$ and the late-time total flux into the well is approximated by

$$q_L \simeq \frac{\tilde{a}}{\beta}(1 + KH)\left(\frac{1}{t}\right)^{1/2}, \tag{4.4}$$

where, after the pressure equilibration, the lateral extent of rock which has decompressed scales as $L_D \sim \beta t^{1/2}$. The parameter β can now be determined from the asymptotic form of the mass conservation principle:

$$\phi \int_0^{L(t)} \rho \, \mathrm{d}x = \int_0^t q \, \mathrm{d}t, \quad \text{with} \quad t \gg H^2/K \tag{4.5}$$

leading to the relation

$$\beta^2 = \frac{1 + KH}{1 + H} \tag{4.6}$$

and the late-time flux

$$q_L \simeq \tilde{a}(1 + KH)^{1/2}(1 + H)^{1/2} t^{-1/2}. \tag{4.7}$$

In order to illustrate the above scaling laws, we have considered a test problem based on a model with two layers, of thickness and diffusivities ratios $H = 2.5$ and $K = 0.04$, respectively. We also considered $p(0, t) = 0.5$. Then from (4.2) the flux ratio $q_{E1}/q_{E2} \cong 2$ for $t \ll H^2/K$ and from (4.3) the flux ratio $q_{L1}/q_{L2} \cong 10$ for $t \gg H^2/K$. The actual values of the early and late flux can also be calculated using relations (4.1) and (4.7), respectively. The transition of the flux from the early to the late values can be illustrated by the numerical solution of the two-dimensional nonlinear diffusion equation (1.1). We have employed a finite-difference procedure which consists of operator splitting and using a generalization of the Crank–Nicolson method for nonlinear diffusion in each space dimension (Press *et al.* 1992). A constant-pressure boundary condition was imposed on the well side of the domain while on the remaining sides we have imposed no-flow conditions. The infinite horizontal geometry was dealt with by taking the length L of the domain large enough for the time taken for the averaged pressure at $x = L/2$ by to decrease 2 % to be larger than any other time of interest.

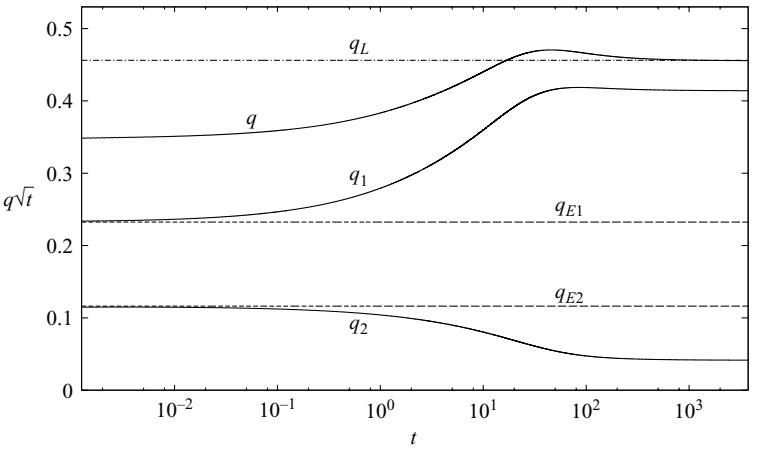

FIGURE 4. The numerical individual-layer and total fluxes (——) compared with the calculated values for the early individual-layer fluxes (— —) and the late total flux (— · —·) for $H = 2.5$, $K = 0.04$ and $p(0) = 0.5$. All fluxes are scaled with $\sqrt{t}$.

Figure 4 shows the numerical prediction for the fluxes for the two layers and the numerical prediction of the total flux, compared with the values calculated using (2.13) for both layers and the value of the late flux calculated using (4.7).

It can be seen in figure 4 that at early stages, as expected, the flux coming from each layer is approximated very well by considering them as independent and using the methodology from the previous section. However, at longer times, since the gas tends to diffuse faster from the high-permeability layer, a pressure gradient is created across the two layers which drives an influx of gas from the low-permeability layer into the high-permeability one. Consequently, the flux issuing from the high-permeability layer is higher than in the case when the layers are independent, e.g. when a seal is present between them. Also, the flux from the low-permeability layer is lower than in the case of independent layers, but the overall effect on the total flux is still an increase because the gas from the low-permeability layer effectively short-circuits the reservoir by flowing into the high-permeability layer. This increase of the total flux relative to the case of two independent layers continues until the pressure equilibration is achieved across the two layers. It can be seen from figure 4 that at this later stage the total flux is very well approximated by relation (4.7).

In order to understand the relation between the time needed for the pressure to equilibrate across the two layers and the parameters of the reservoir we have numerically investigated a few more test problems. The results from these investigations are illustrated in figure 5.

In the first instance, we have taken three different values for permeability ratio $K \in \{1/10, 1/25, 1/90\}$ and six values for the thickness ratio $H \in \{1/4, 1/2, 3/4, 1, 2, 3\}$. In each case we have calculated the time when scaled total flux $q_T\sqrt{t}$ is maximum, which is just before the equilibration is reached, and plotted them against the diffusion time across the lower-permeability layer. The results displayed in figure 5(a) suggest that the equilibration time scales as $t_{max} \sim H^2/K$. This scaling law was then tested in a second set of numerical tests for a more extensive range of parameters $K \in \{0.1, 0.01, 0.001\}$ and $H \in \{1, 10, 100\}$. Figure 5(b) shows the numerical fluxes, which are scaled with the corresponding early flux q_E in each case, against the scaled time tK/H^2. These

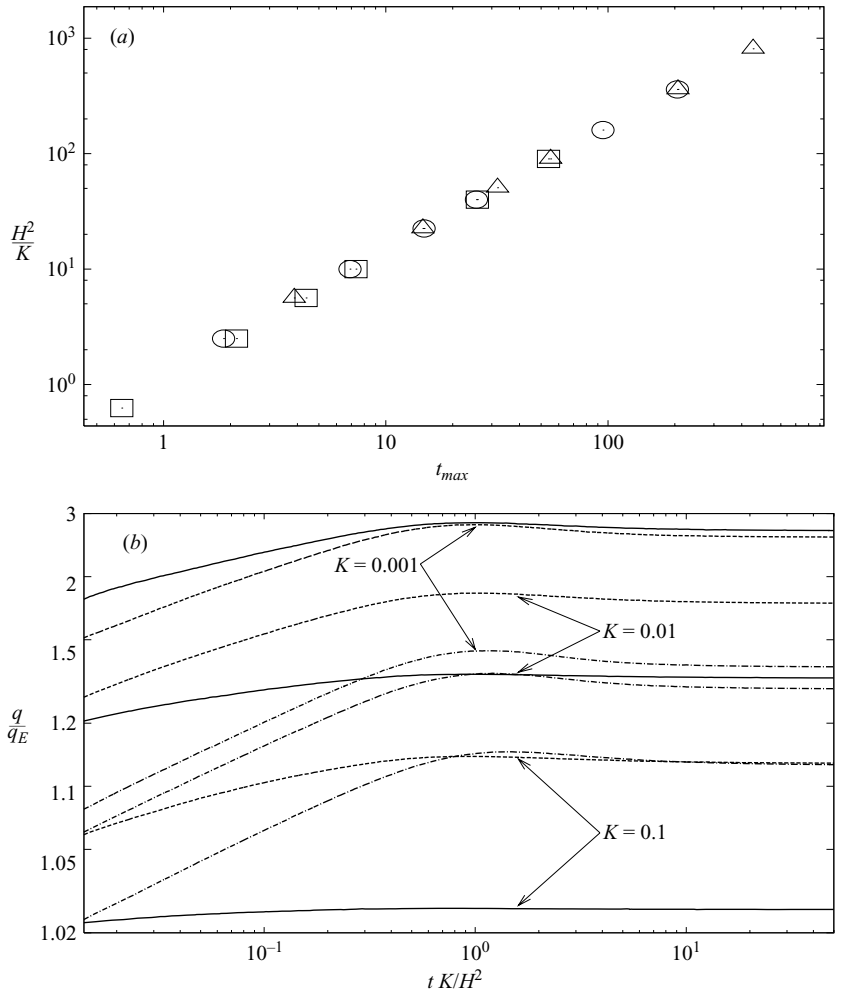

FIGURE 5. (*a*) Time when $q\sqrt{t}$ reaches maximum for $H \in \{1/4, 1/2, 3/4, 1, 2, 3\}$, $K = 1/10$ (□), $K = 1/40$ (○) and $K = 1/90$ (△). (*b*) The numerical total fluxes for test problems with $H = 100$ (——), $H = 10$ (— — —), $H = 1$ (— · —·) and $K = 0.001$ (top), $K = 0.01$ (middle), $K = 0.1$ (bottom). In all cases the fluxes are scaled with the corresponding early flux q_E, and the time is scaled with H^2/K.

results show that $t_{max}K/H^2 \simeq 0.9$. Therefore, the equilibration time scales with the diffusion time across the lower-permeability layer.

Using (4.1) and (4.7) the ratio of the late-time versus early-time flux is given by

$$\frac{q_L}{q_E} \simeq \frac{(1 + KH)^{1/2}(1 + H)^{1/2}}{1 + K^{1/2}H}. \tag{4.8}$$

The flux ratio (4.8) is in fact a measure of the advantages of the inter-layer gas flow in the coupled model compared with the gas flow in an independent-layer model. Figure 6 shows the values of the ratio (4.8) for several values of the permeability ratios K and a window of ratios of layer thicknesses H. It can be seen in figure 6 that, as expected, a very thin low-permeability layer, i.e. $H \ll 1$, has a negligible impact on the coupled flux, because the low-permeability layer contains only a limited mass of

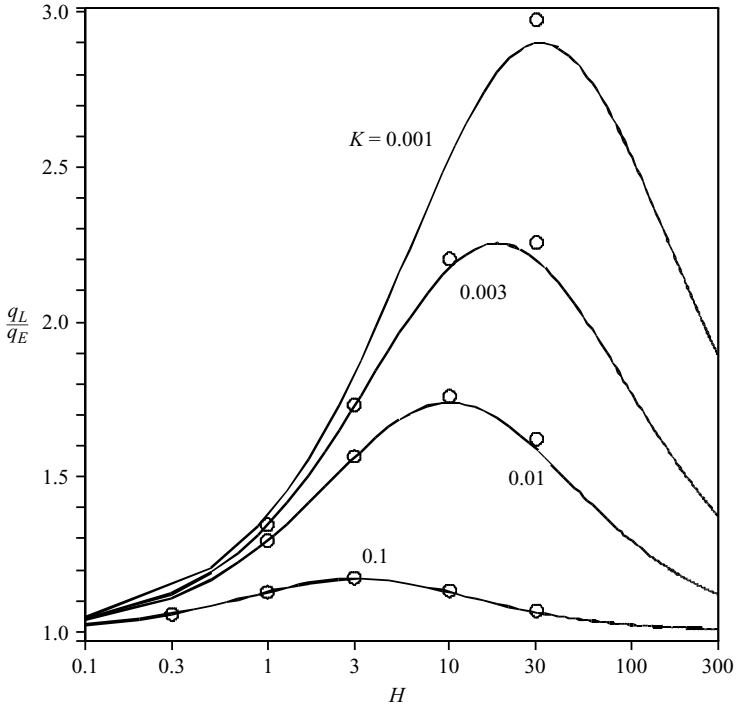

FIGURE 6. The flux ratio q_L/q_E for several values of the permeability ratios K and a window of ratios of layer thicknesses H. The theoretically calculated values (——) are compared to numerical results (○).

gas. As H increases, there is a sizeable increase of the flux ratio, owing to a major flow of gas from the low- to the high-permeability layer. The maximum effect occurs when the thicknesses ratio $H = 1/\sqrt{K}$. The value of this maximum is

$$\frac{q_L}{q_E}(H = 1/\sqrt{K}) = \frac{1}{2}\sqrt{2 + \sqrt{K} + 1/\sqrt{K}}. \tag{4.9}$$

Thus for $K \ll 1$ the maximum flux ratio can be approximated as $q_L/q_E \simeq 0.5K^{-1/4}$ and the importance of the inter-layer gas flow becomes greater as the contrast between the permeabilities of the two layers increases. The importance of this inter-layer flux also increases with thickness ratio H up to a critical value of the low-permeability layer. However if the low-permeability layer is very thick compared to the high-permeability layer, such that $H \gg 1/\sqrt{K}$, then the impact of the coupling is again of reduced importance. In this limit high-permeability streaks do not greatly increase the flow, as most of the gas in the low-permeability layer continues to flow through the low-permeability layer.

4.2. *Bounded domain*

We consider now two layers having length L, thicknesses h_1 and h_2, permeabilities k_1 and k_2 and corresponding diffusion coefficients α_1 and α_2, respectively. As in the unbounded-domain case, we non-dimensionalize all the quantities of interest, including now the length L, with the choice of the first layer as the reference layer.

4.2.1. *Pressure equilibration between the layers*

If we assume that the pressure equilibration between the layers is achieved before the end effects become significant, then from the same considerations as in § 2.1, the late-time flux in the limit case when $P_0 = P(0, t) = 0$ is approximated by

$$q_{equil} = a(1 + KH)\left[\frac{f(0)}{1 + cf(0)(\overline{\alpha}/L^2)t}\right]^2 \tag{4.10}$$

where $\overline{\alpha} = \beta^2 = (1 + KH)/(1 + H)$.

We have seen in § 4.1 that the time needed for pressure equilibration between the layers is related to the time at which the scaled total flux $q_T\sqrt{t}$ is maximum. This time t_{max} scales with the diffusion time across the lower-permeability layer and in § 4.1 we found $t_{max} \simeq 0.9H^2/K$. On the other hand, the end effects become important when the pressure signal has reached the far end of the reservoir. A lower bound for this time is given by the diffusion time along the reservoir through the high-permeability layer 1, $t_{D1} \sim L^2$. Thus relation (4.10) should be a good approximation for the late-time flux if $t_{D1} > t_{max}$. This inequality may be recast as

$$K\frac{L^2}{H^2} > c_{equil}, \tag{4.11}$$

where the value of the constant c_{equil} is determined by the scaling factors in the relations for t_{max} and t_{D1}. With the relations found in § 2 and § 4.1, namely $t_{D1} \simeq 0.15L^2$ and $t_{max} \simeq 0.9H^2/K$, we have $c_{equil} \simeq 6$.

It should be noted however that the pressure signal along the high-permeability layer is delayed by the gas issuing into this layer from the low-permeability one. Therefore condition (4.11) is likely to be too restrictive, especially in the case of a high-permeability streak ($H \gg 1$). If pressure equilibration between the layers takes place, it implies that the flux from the low-permeability layer from into the high-permeability one is greater than the maximum flux of the high-permeability layer into the well. As these two fluxes scale with KL/H and $1/L$, respectively, the equilibration condition can be written as

$$\sqrt{K}\frac{L^2}{H} > c_{equil}. \tag{4.12}$$

Figure 7(a) presents a comparison between the theoretical late-time equilibrium flux q_{equil} and the numerical flux for several reservoirs having $p_0 = p(0, y, t) = 0.01$, $H = 1$, $K = 0.1$, and decreasing lengths $L = 40$, $L = 20$, $L = 10$, $L = 6$ and $L = 4$. The numerical fluxes were computed in the time interval when the maximum pressure in the reservoirs drops from 0.95 to 0.02, i.e. from the moment when the end effects become significant until the reservoir is about 99 % depleted. Figure 7(b) presents the results of similar calculations for reservoirs with $L = 40$ and increasing lengths $H = 1$, $H = 5$, $H = 10$ and $H = 20$. If we denote

$$\gamma = K\frac{L^2}{H} \tag{4.13}$$

then for the cases considered in figure 7(a), γ has the values 160, 40, 10, 3.6, and 1.6. It can be observed from figure 7 that when $\gamma > c_{equil}$, i.e. when $L \in \{10, 20, 40\}$, the relative difference between the theoretical flux q_{equil} and the numerical flux q_{num} is less than 2 % in most of the time interval considered, except near the beginning, where the flux adjusts from the previous regime, and close to the end, where the numerical solution departs from the separable prediction. This discrepancy at long time is a

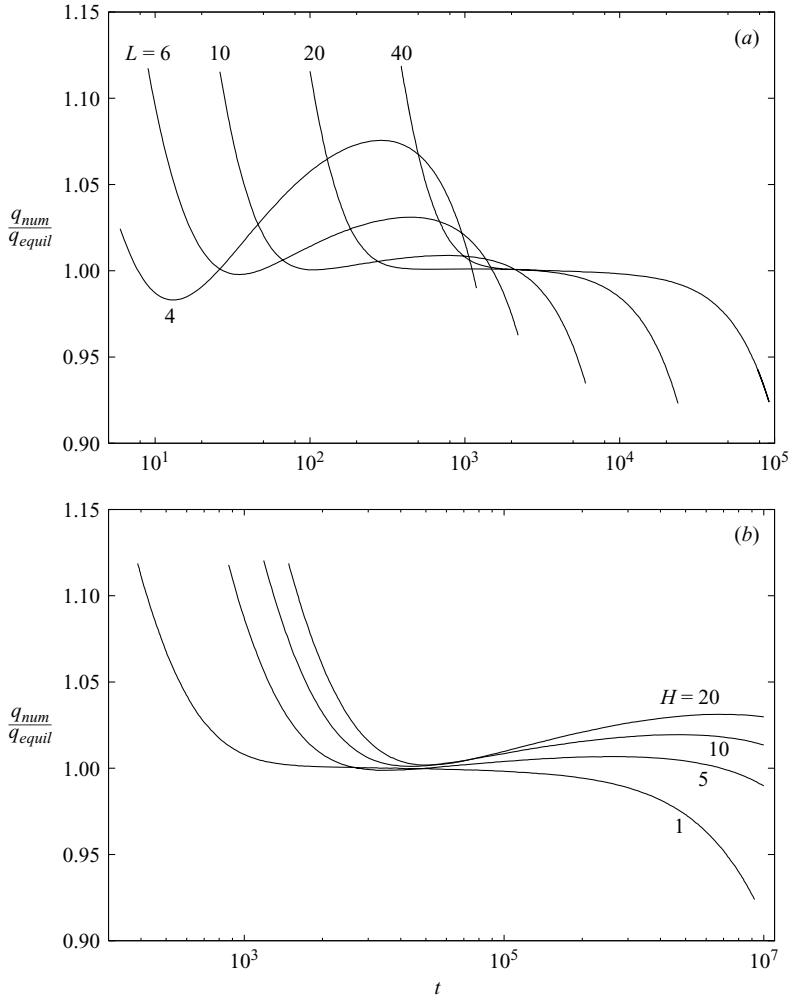

FIGURE 7. The ratio between the numerical flux q_{num} and the theoretical late equilibrium flux q_{equil} for two-layer bounded reservoirs with $p_0 = 0.01$, $K = 0.1$, and (*a*) $H = 1$, and $L \in \{4, 6, 10, 20, 40\}$, and (*b*) $L = 40$ and $H \in \{1, 5, 10, 20\}$.

result of the non-zero fracture pressure p_0 considered in the simulation, i.e. $p_0 = 0.01$, which contrasts with the analytical solutions where we assume that $p_0 = 0$. However, even with $L = 4$ when $\gamma \simeq 0.25 c_{equil}$, the maximum difference between the two fluxes is only about 7 % in the time interval considered. In the case of figure 7(*b*), γ has the values 160, 32, 16 and 8 and the difference between q_{equil} and q_{num} is again less than 2 % in most of the time interval considered.

4.2.2. *No pressure equilibration between the layers*

We consider now the situation when $\gamma = KL^2/H \ll c_{equil}$. The simplest case is $0 \ll K < 1$. Then it follows that $L \ll H$, which means that the interface between the layers has a much smaller area than the area of intersection between the layers and the fracture. This may be the case in a faulted system in which gas flows through the fault fracture from a localized block (figure 8*a*). Together with the fact that the discrepancy between the permeabilities of the two layers is not very big, it follows

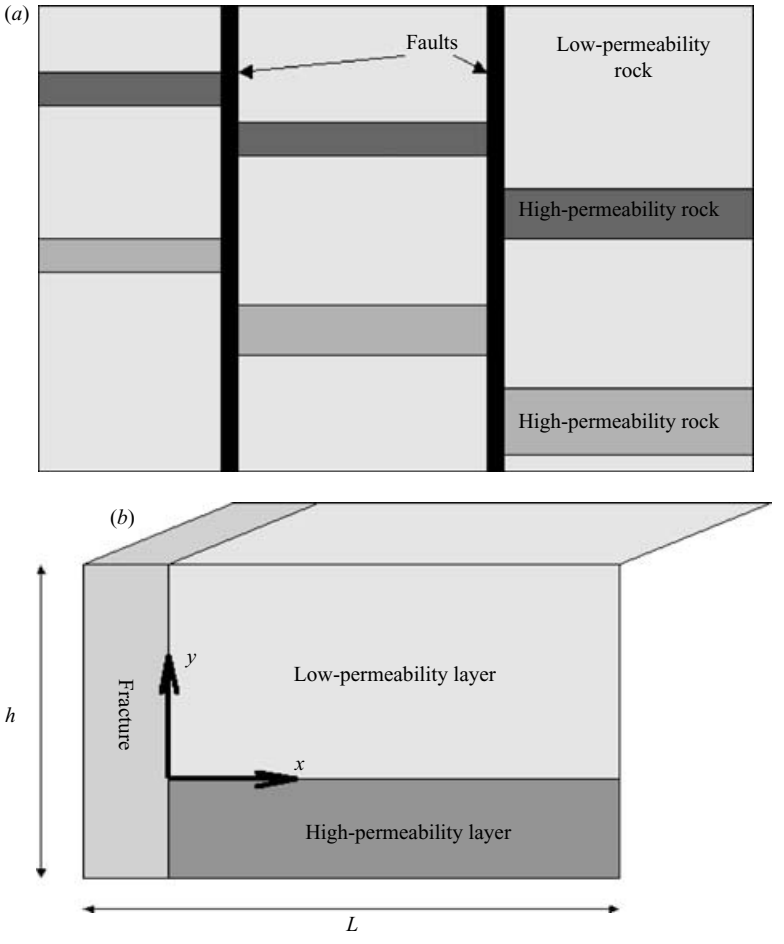

FIGURE 8. Schematic of (*a*) a faulted system, (*b*) a localized bloc in the faulted system.

that there will be little inter-layer flow and most of the gas will flow directly into the fracture. Therefore in this case the sum of two independent separable solutions describes the process.

A second case is when $0 < K \ll 1$. In this situation, it is even possible that $L/H > 1$ and thus the inter-layer gas flow cannot be neglected. However, as the diffusion time along a layer scales with its permeability, it follows that the first layer will decompress much faster than the second one. It can be then expected that an initial extraction period when the production is driven by the depletion of the first layer will be followed by a second stage when the gas from the second layer will flow both directly into the fracture and also into the, now almost totally decompressed, first layer. It is thus relevant to briefly consider the simplified problem when gas flows from a reservoir with length L, width h and diffusion coefficient α both into the fracture and into a very high-permeability layer beneath in which the pressure is also p_0. The extraction of gas is now expressed by the two-dimensional equation

$$p_t - \alpha(pp_x)_x - \alpha(pp_y)_y = 0, \tag{4.14}$$

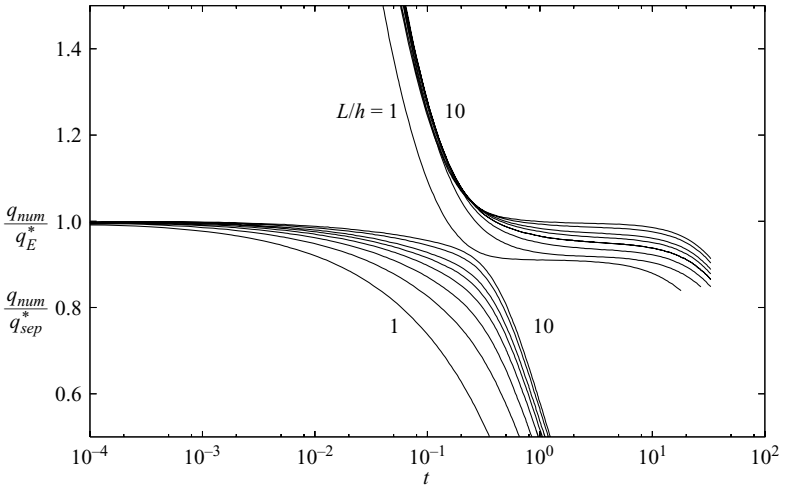

FIGURE 9. The ratios between the numerical flux q_{num} and the theoretical fluxes q_E^* and q_{sep}^* for several reservoirs with $L/h \in \{1, 2, 3, 4, 5, 6, 8, 10\}$, $\alpha = 0.1$ and $h = 0.1$. The gas is draining into a lateral fracture of length h and a bottom fracture of length L at pressure $p_0 = 0.01 p_{max}$.

where α, p are as in (2.3), and y denotes the distance normal to the interface between the layers (figure 8*b*). The boundary conditions are now

$$p(0, y, t) = p(x, 0, t) = 0 \qquad \text{and} \qquad \frac{\partial p}{\partial x}(L, y, t) = \frac{\partial p}{\partial y}(x, h, t) = 0. \tag{4.15}$$

It should be noted that in this two-dimensional nonlinear case, the governing equation (4.14) no longer admits a complete separation of variables in the limit case when $p_0 = 0$. It is possible to perform a partial separation however, namely

$$p(x, y, t) = f^*(t) g^*(x, y) \tag{4.16}$$

and it follows that

$$f_{c^*}^*(t) = \frac{f_{c^*}^*(0)}{1 + c^* \alpha t}, \tag{4.17}$$

where c^* depends on L and h.

Based on (4.17) we propose the following empirical formula for the separable flux q_{sep}^*:

$$q_{sep}^* \simeq \alpha \left(\frac{h}{L} + \frac{L}{h} \right) \frac{c_1}{[1 + c_2 \alpha (1/L^2 + 1/h^2) t]^2}. \tag{4.18}$$

An upper bound for the flux at early stages can be given by a relation similar to (2.13):

$$q_E^* \simeq \tilde{a}(h + L) \left(\frac{\alpha}{t} \right)^{1/2}. \tag{4.19}$$

Figure 9 presents a comparison between the theoretical fluxes q_E^* and q_{sep}^*, and the numerical flux q_{num} for reservoirs having aspect ratios L/h from 1 to 10. The other parameters of the reservoirs are $p_0 = 0.01$, $\alpha = 0.1$ and $h = 0.1$. The coefficients c_1 and c_2 are here 1.12 and 1.3, respectively. Although (4.18) is not an exact relation, the model's predictions are within 5 % of the numerical calculations. It should be noted that for reservoirs with very large aspect ratio, i.e. $L/h \gg 1$, the flow is

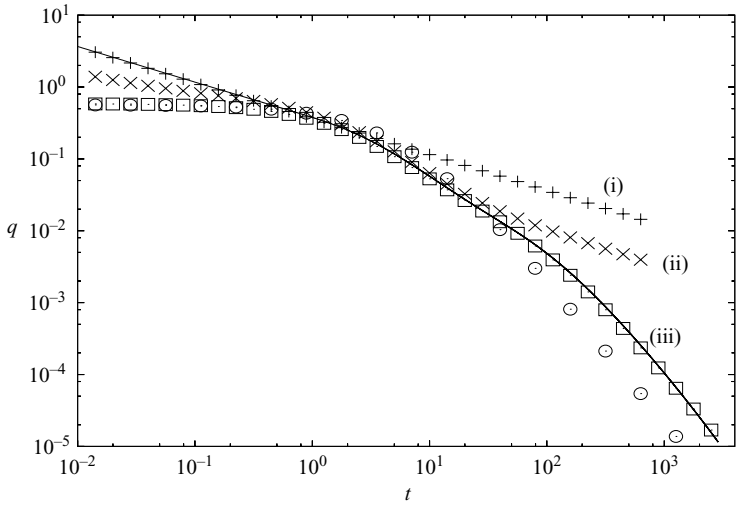

FIGURE 10. The numerical flux (——) obtained for a two-layer bounded reservoir with $p_0 = 0.01$, $H = 1$, $L = 2$, $K = 0.01$, compared to the sum of the early individual layer fluxes $q_{E1} + q_{E2}$ (+ + +), the theoretical late equilibrium flux q_{equil} (○ ○ ○), and theoretical sums $q_{sep1} + q^*_{E2}$ (× × ×) and $q_{sep1} + q^*_{sep2}$ (□ □ □). (i)–(iii) denote flow regimes described in the text.

essentially one-dimensional and the prediction of formula (4.18) should coincide with the prediction of (2.10). Thus, for $L/h \gg 1$, the best-fit values for the coefficients c_1 and c_2 should converge towards $af(0)^2 \simeq 1.12$ and $cf(0) \simeq 1.27$, respectively. However, for the moderate range of aspect ratios considered here, i.e. $1 \leqslant L/h \leqslant 10$, the choice $c_2 = 1.3$ provides a better estimate of the numerical fluxes.

Let us now go back to the two-layer case. We consider a test example with $p_0 = 0.01$, $H = 1$, as in the previous examples, but now we take $K = 0.01$ and $L = 2$. With these parameters we have $\gamma = 0.04$ which is about 100 times lower than the equilibration constant c_{equil} and therefore the equilibration between the layers should not be achieved and, furthermore, the high-permeability layer will be almost totally decompressed before the end effects become important in the low-permeability layer. The numerical flux q_{num} obtained for this example is displayed in figure 10.

It can be seen that, as expected, at early times there are big discrepancies between q_{num} and the theoretical late-time equilibrium flux q_{equil}. During the interval $0 < t_{D1}$ ($t_{D1} \simeq 0.15L^2 = 0.6$) needed for decompression to start at the end of high-permeability layer, the numerical flux is approximated well by the sum of the individual early fluxes in the two layers, namely $q_{E1} + q_{E2}$. This initial flow regime (i), is followed by a second regime (ii) when the end effects are present in the high-permeability layer 1, but still not in the low-permeability layer 2, i.e. for $t_{D1} < t < 0.15 \min\{H^2/K, L^2/K\}$. In this regime, an upper bound for the flux is given by the sum of the separable prediction for layer 1, q_{sep1}, from equation (2.10) and the early flux q^*_{E2} of layer 2, from equation (4.19). In the final flow regime (iii), when the end effects are present in both layers, i.e. $t > 0.15 \min\{H^2/K, L^2/K\} = 60$, an upper bound for the flux is given by the sum of the separable flux of the first layer, q_{sep1}, and the partially separable flux from the second layer, q^*_{sep2}, which was calculated according to (4.18). It can be seen from figure 10 that the numerical flux adjusts very quickly to $q_{sep1} + q^*_{sep2}$ for $t > 60$.

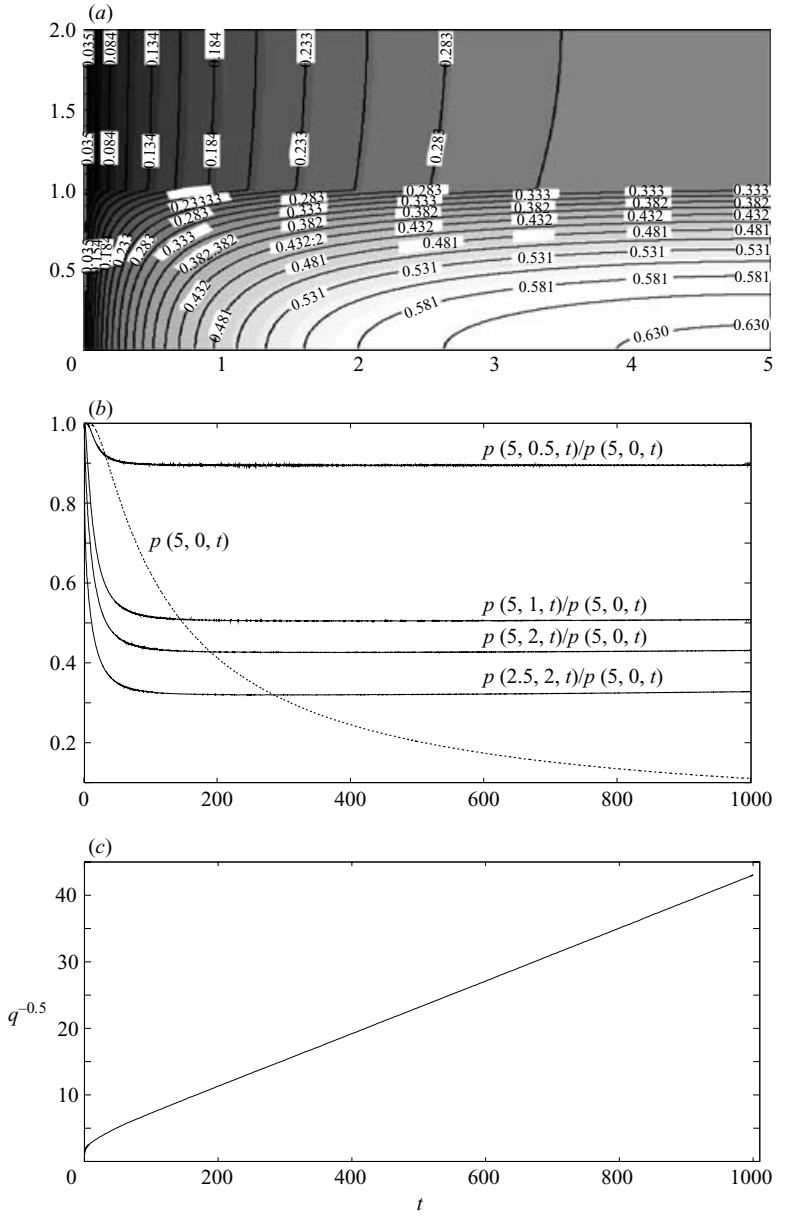

FIGURE 11. The numerical results obtained for a two-layer bounded reservoir with $p_0 = 0.01$, $H = 1$, $L = 5$, $K = 0.01$: (*a*) the pressure distribution at $t = 100$, (*b*) variation of pressure at $(x, y) = (5, 0)$ $(\cdot\ \cdot\ \cdot)$ and the variation of the ratios between the pressure at locations $(5, 0.5)$, $(5, 1)$, $(5, 2)$, $(2.5, 2)$ and the pressure at $(5, 0)$, and (*c*) the variation of $1/\sqrt{q_{num}}$.

We discuss now the case when $0 \ll \gamma < c_{equil}$. This means that the pressure equilibration between the layers still does not occur but in the same time the high-permeability layer is no longer almost decompressed after the initial stages of production, as in the previous case. A typical example is illustrated in figure 11, which presents the results obtained for a reservoir with $p_0 = 0.01$, $H = 1$ and $K = 0.01$, as in the previous example, but now with $L = 5$ ($\gamma = 0.25$). Figure 11(*a*) shows the

pressure distribution in the reservoir at $t = 100$, which is after the end effects have started in both layers. It can be seen that the average pressure at the far end of the high-permeability layer is approximately half the value of the maximum pressure in the reservoir, and the flow is fully two-dimensional. Figure 11(b) shows the variation of the maximum pressure in the reservoir and the variations of the pressure at four different locations on the boundary relative to the maximum pressure. It can be observed these pressure ratios quickly become constant after the start of the end effects. This indicates that the solution in this case is still separable with respect to the time variable. Finally, in figure 11(c) we have plotted the quantity $1/\sqrt{q_{num}}$, where q_{num} is the total flux into the well. As expected this quantity quickly adjusts to a linear variation. Even without an analytical expression for the flux this property allows the prediction of the future flow rate based on the production history in real situations.

5. Summary

We have presented a series of models to describe the extraction of gas at constant pressure from a stratified porous reservoir, including the end effects due to the finite length of the reservoir. Simple scalings laws developed to determine the fluxes into the fracture, and the length scales and time scales associated with the nonlinear diffusion process have been validated using numerical simulations. In the first approximation, we have considered unbounded reservoirs consisting of one or two layers of different thickness and permeability. The one-layer case admits a simple similarity solution which implies that the fracture flux scales as $q \sim h\sqrt{\alpha/t}$ where h and α are the thickness and the diffusivity of the layer. In the two-layer case an initial stage when the diffusion processes in the two layers can be considered as independent of each other is followed by a stage when the gas from the low-permeability layer short-circuits to the fracture along the high-permeability layer. This results in an increased total flux when compared to an independent layer situation and, allowing sufficient lateral extent of the reservoir, then the pressure across the two layers gradually equilibrates. Based on this we have determined a law for the late-time flux. We have also found that the equilibration time scales with the diffusion time across the lower-permeability layer and we have given a formula for calculating the benefit of inter-layer gas flow.

We then investigated the end effects due to the finite length L of the reservoir, which become important for $t > t_D$, where t_D scales with the diffusion time along the reservoir. When a constant pressure is specified as the initial condition, the fracture flux switches from the similarity solution to the separable solution at $t_D \approx 0.15L^2/\alpha$. For the two-layer case, we have determined a law for the flux when pressure equilibration is achieved between the layers. We have seen that this law gives a good approximation for the late-time flux when $\gamma (= KL^2/H) > c_{equil} \approx 6$, i.e. when the diffusion time along the reservoir is comparable with or larger than the diffusion time across the lower-permeability layer. We have then discussed the situation when $\gamma \ll c_{equil}$ and therefore there is no pressure equilibration between the layers. We have shown that the case $0 < K \ll 1$ can be approximated to a problem of gas flowing from the lower-permeability layer both into the fracture and into the higher-permeability layer which is assimilated into a fracture. This problem admits a partially separable solution and we have shown on a numerical example that after the end effects become important, the total flux adjusts very quickly to the sum of the separable flux of the high-permeability layer and the partially separable flux from the low-permeability layer.

We thank BP, Shell, BG, Conoco Phillips, Total, Chevron, DTI and ITF for sponsorship and support of this project.

REFERENCES

Aronson, D. G. & Peletier, L. A. 1981 Large time behaviour of solutions of the porous medium equation in bounded domains. *J. Diffl Equat*. **39**, 378–412.

Barenblatt, G. I. 1996 *Scaling, Self-Similarity, and Intermediate Asymptotics*. Cambridge University Press.

Barenblatt, G. I., Entov, V. M. & Ryzhik, V. M. 1990 *Theory of Fluid Flows Through Natural Rocks*. Kluwer.

Bear, J. 1972 *Dynamics of Fluids in Porous Media*. Dover.

Boussinesq, J. 1904 Recherches theoriques sur l'ecoulement des nappes d'eau infiltrees dans le sol et sur debit de sources. *C. R. H. Acad. Sci, J. Math. Pures Appl.* **10**, 5–78 and 363–394.

Dagan, G. 1989 *Flow and Transport in Porous Formations*. Springer.

King, S. E. & Woods, A. W. 2003 Dipole solutions for viscous gravity currents: theory and experiments. *J. Fluid Mech.* **483**, 91–109.

Leibenzon, L. S. 1929 Gas movement in a porous medium. *Neft. i Slants. Khoz*. **10**, 497–519 (in Russian).

Muskat, M. & Botset, H. G. 1931 Flow of gases through porous materials. *Physics* **1**, 27–47.

Press, W. H., Teukolsky, S. A., Vetterling, W. T. & Flannery, B. P. 1992 *Numerical Recipes in Fortran 77*. Cambridge University Press.

Shestakov, V. M. 1956 Some problems of modelling. In *Voprosy Filtratsionnykh Raschetov Gidrotekhnicheskikh Sooruzheniy*, pp. 129–139. Gosstroyizdat, Moskow (in Russian).